REVISTA DE CIÊNCIAS EXATAS E TECNOLOGIA

DUAL BOUNDARY ELEMENT METHOD TO DETECT THE PRESENCE OF CRACKS USING DYNAMIC STRAIN DETERMINATION FOR HEALTH MONITORING

Sandro Petry Laureano Leme – *Centro Universitário Anhanguera de Campo Grande*

ABSTRACT: The present paper is concerned with the application of the Dual Boundary Element Method in dynamics for the determination of the strain in plates subject an external impact load. The use of the Laplace Transform in the boundary element method allows us to determine with precision the values of the strain inside the structure under study for each frequency selected. This precisely strain determination, together with the formulation of the couple piezoelectric effect for the sensor used, possibly the proposal of a new methodology of health monitoring of structures dynamically loaded.

KEYWORDS:
dual boundary element method, health monitoring of structures dynamically loaded

Artigo Original
Recebido em: 30/10/2009
Avaliado em: 14/02/2014
Publicado em: 28/04/2014

Publicação
Anhanguera Educacional Ltda.

Coordenação
Instituto de Pesquisas Aplicadas e Desenvolvimento Educacional - IPADE

Correspondência
Sistema Anhanguera de Revistas Eletrônicas - SARE
rc.ipade@anhanguera.com

1. INTRODUCTION

Thin plate structures are widely used in analysing engineering structures (Wen at all, 2000). The dynamic analysis is sometimes more precisely than the static one and for some cases must be employed rather than the static analysis. The applications of boundary element method to the dynamic analysis for plate bending problem were presented by Bezin (1991). A comprehensive description of recent advances in BEM in plate bending can be found in Ref. (Aliabadi, 1998).

The application of the dynamic equations to isolate beams together with the DBEM in the Laplace Domain allow us to evaluate the behaviour of stiffened structure when they are subjected a dynamic loads. This paper intends to show the use of the Dual Boundary Element Method with dynamic loads in stiffened plates for the determination of cracks inside the plate.

First it will be derived the equations to the lateral and longitudinal vibration of an isolated beam under an external harmonic load, which will be used to predict the deformation inside the piezoelectric sensors used to determine the presence of cracks. Then with the use of some compatibility consideration it will be developed the equations of motions of the internal points of the plate with the presence of these sensors.

2. DUAL BOUNDARY ELEMENT METHOD USING LAPLACE TRANSFORM FOR DYNAMIC ANALYSIS

The general field equation for elastodynamics, may be written as (Domingues, 1993):

$$c_1^2 \nabla\nabla u - c_2^2 \nabla x \nabla x u - \frac{\partial^2 u}{\partial t^2} = -b \tag{1}$$

where $c_1=(\lambda+2\mu/\rho)^{1/2}$ is the P-wave velocity; $c_2=(\mu/\rho)^{1/2}$ is the S-wave velocity; λ and μ are the Lame constants; ρ is the density; and ρb is the body force vector and u is the displacement vector.

For 2 D dynamic problems the fundamental solutions are:

$$U_{ij} = \frac{1}{2\pi\rho c_2^2}\left[\psi\delta_{lk} - \chi\, r_{,l}\, r_{,k}\right] \tag{2}$$

$$T_{ij} = \frac{1}{2\pi}\left[\left(\frac{d\psi}{dr} - \frac{1}{r}\chi\right)\left(\delta_{lk}\frac{\partial r}{\partial n} + r_{,k}n_{,l}\right) - \frac{2}{r}\chi\left(n_{,k}\, r_{,l} - 2r_{,l}\, r_{,k}\frac{\partial r}{\partial n}\right) - 2\frac{d\chi}{dr}r_{,l}\, r_{,k}\frac{\partial r}{\partial n} + \ldots\right.$$
$$\left. \ldots + \left(\frac{c_1^2}{c_2^2} - 2\right)\left(\frac{d\psi}{dr} - \frac{d\chi}{dr} - \frac{1}{r}\chi\right)r_{,l}\, n_{,k}\right] \tag{3}$$

The value for the functions Ψ and χ for the 2D analysis are given in the appendix.

The Dual Boundary Element Method (DBEM), as presented by Portela et al. (Portela et al, 1992), is capable of analysing configurations involving any number of edges and embedded cracks in any given geometry. The need for dividing the problem in different regions, common to many boundary element formulations, is avoided by using the displacement equation when collocating at one crack surface and the dual traction equation when collocating at the other crack surface (Salgado et al., 1996). The use of Laplace Transform enables us to have a simpler way to analyse the problem and to achieve reasonable answers for dynamic analysis.

The boundary integral displacement equation, for a source point x' at the boundary Γ of a finite sheet is give by:

$$c_{ij}(x')\,u_j(x') + \int_\Gamma T_{ij}(x',x)\,u_j(x)\,d\Gamma(x) = \int_\Gamma U_{ij}(x',x)\,t_j(x)\,d\Gamma(x)\ldots$$
$$\ldots + \iint_\Omega U_{ij}(x',X)\,b_j(X)\,d\Omega(X) \qquad (4)$$

where $T_{ij}(x',x)$ and $U_{ij}(x',x)$ are the Kelvin traction and displacement fundamental solutions, respectively, $u_j(x)$ and $t_j(x)$ are the displacements and tractions at boundary field points x, $b_j(X)$ are body forces acting at field points X inside the domain Ω and c_{ij} is a coefficient that can be determined by rigid body movement considerations.

The corresponding traction boundary integral equation, presented below, can be obtained by differentiation of equation (4), application of the Hooke's law and multiplication by the outward normal,

$$\frac{1}{2}t_j(x') + n_i(x')\int_\Gamma S_{ijk}(x',x)\,u_k(x)\,d\Gamma(x) = n_i(x')\int_\Gamma D_{ijk}(x',x)\,t_k(x)\,d\Gamma(x)\ldots$$
$$\ldots + n_i(x')\iint_\Omega D_{ijk}(x',X)\,b_k(X)\,d\Omega(X) \qquad (5)$$

where $S_{ijk}(x',x)$ and $D_{ijk}(x',x)$ contain derivatives of $T_{ij}(x',x)$ and $U_{ij}(x',x)$, respectively and $n_i(x')$ denotes the *i-th* component of the unit outward normal to the boundary at the source point x'. The plate is considered to be thin, so that the interactions forces exchanged with the stiffeners can be treated as action-reaction body forces. The plate displacement and traction equations can be derived by considering equations (4) and (5) which assume the presence of body forces. If, instead of being distributed over the whole domain, the body forces are confined to straight lines inside it, the domain integrals in equations (4) and (5) reduce to line integrals over the body forces loci. The displacement and traction equations for a thin plate with N stiffeners continuously bonded to it can thus be written as:

$$c_{ij}(x')\,u_j(x')+\int_\Gamma T_{ij}(x',x)\,u_j(x)\,d\Gamma(x)=\int_\Gamma U_{ij}(x',x)\,t_j(x)\,d\Gamma(x)\ldots$$
$$\ldots+\frac{1}{h}\sum_{n=1}^{N}\int_{\Gamma_{Sn}} U_{ij}(x',X)\,b_j^{\,Sn}(X)\,d\Gamma_{Sn}(X) \qquad (6)$$

and

$$\frac{1}{2}t_j(x')+n_i(x')\int_\Gamma S_{ijk}(x',x)\,u_k(x)\,d\Gamma(x)=n_i(x')\int_\Gamma D_{ijk}(x',x)\,t_k(x)\,d\Gamma(x)\ldots$$
$$\ldots+n_i(x')\frac{1}{h}\sum_{n=1}^{N}\int_{\Gamma_{Sn}} D_{ijk}(x',X)\,b_k^{\,Sn}(X)\,d\Gamma_{Sn}(X) \qquad (7)$$

where Γ_{Sn} stands for the stiffeners loci, b_k^{Sn} represents the unknown sensor attachment forces and h is the plate thickness.

3. DISPLACEMENT COMPATIBILITY

The displacement compatibility conditions for points at the stiffeners attachment region are based on the assumption that the displacement u_j of a point X' ($X' \in \Gamma_{sn}$) at the plate and u_j^{Sn} of a corresponding point at the *n-th* stiffener, has to be compatible with the shear deformation of the adhesive layer connecting the sensor to the plate. They are expressed, with respect to a reference point X^0 at the same sensor locus ($X^0 \in \Gamma_{sn}$), by N sets of relations as:

$$\Delta u_j(X')-\Delta u_j^{\,Sn}(X')=\frac{h_{Ad}}{G_{Ad}}\Delta\tau_j^{\,Ad}(X') \qquad (8)$$

where h_{Ad} is the thickness of the adhesive layer, G_{Ad} is the coefficient of shear deformation of the adhesive material, τ_j^{Ad} is the shear stress at the adhesive, $\Delta u_j(X') = u_j(X')-u_j(X^0)$, $\Delta u_j^{Sn}(X') = u_j^{Sn}(X')-u_j^{Sn}(X^0)$, $\Delta\tau_j^{Ad}(X') = \tau_j^{Ad}(X')-\tau_j^{Ad}(X^0)$. For the line stiffeners, the adhesive shear stress τ_j^{Ad} are equal in value to the attachment forces b_j^{Sn} divided by the width of the adhesive line w_{Ad}. The displacement compatibility equation can be written in terms of the body forces as:

$$\Delta u_j(X')-\Delta u_j^{\,Sn}(X')=\Phi_{Ad}\Delta b_j^{\,Sn}(X') \qquad (9)$$

where $\Delta b_j^{Sn}(X') = b_j^{Sn}(X')- b_j^{Sn}(X^0)$ and

$$\Phi_{Ad}=\frac{h_{Ad}}{w_{Ad}G_{Ad}} \qquad (10)$$

is the coefficient of shear deformation of the adhesive.

If the reference point X^0 is taken to coincide with the sensor starting point *(y=0)*, the relative displacement Δu_j^{Sn} in equation (9) can be expressed as a function of the unknown interaction forces b_j^{Sn}, which will be determined for the sensors applied in the structure and will be shown in the next section. The relationship between the relative displacements and forces expressed in terms of the plate and the sensors coordinate systems is given by:

$$\Delta u_i^{Sn} = \Theta_{ij}^{Sn} \Delta v_j^{Sn} \tag{11}$$

and

$$b_i^{Sn} = \Theta_{ij}^{Sn} f_j^{Sn} \tag{12}$$

The transformation matrix being:

$$\Theta^{Sn} = \begin{bmatrix} +\cos\varphi^{Sn} & -\sin\varphi^{Sn} \\ +\sin\varphi^{Sn} & +\cos\varphi^{Sn} \end{bmatrix} \tag{13}$$

where φ^{Sn} is the angle between the plate direction x_2 and the *n-th* sensor axis.

The plate relative displacement $\Delta u_j(X') = u_j(X')-u_j(X^0)$ in equation (9) can be then finally written as:

$$\Delta u_j(X') = \int_\Gamma \left[U_{ij}(X',x) - U_{ij}(X^0,x)\right] t_j(x)\, d\Gamma(x) - \int_\Gamma \left[T_{ij}(X',x) - T_{ij}(X^0,x)\right] u_j(x)\, d\Gamma(x) + \ldots$$

$$\ldots + \frac{1}{h}\sum_{n=1}^{N} \int_{\Gamma_{Sn}} \left[U_{ij}(X',X) - U_{ij}(X^0,X)\right] b_j^{Sn}(X)\, d\Gamma_{Sn}(X) \tag{14}$$

The problem can be totally solved by making use of the Equilibrium equations over each stiffener.

For the stiffeners to be in equilibrium, the following equations have to be satisfied:

$$F_1(L) - F_1(0) - \int_0^L f_1(y)\, dy = 0 \tag{15}$$

$$F_2(L) - F_2(0) - \int_0^L f_2(y)\, dy = 0 \tag{16}$$

$$M(L) - M(0) - LF_1(0) = \int_0^L (L-y) f_1(y)\, dy \tag{17}$$

4. SENSORS EQUATIONS

The figure 1(a) shows a plate with some sensors. For low values of the deformations we can consider the problem in 2 dimensions, that means not considering the effects of the out of plane displacements. Also the loads are only applied in the direction x or y given thus the possibility of the 2D analysis for the problem. The considering forces in plate and the forces and momentums in the stiffeners are showed in figure 1(b).

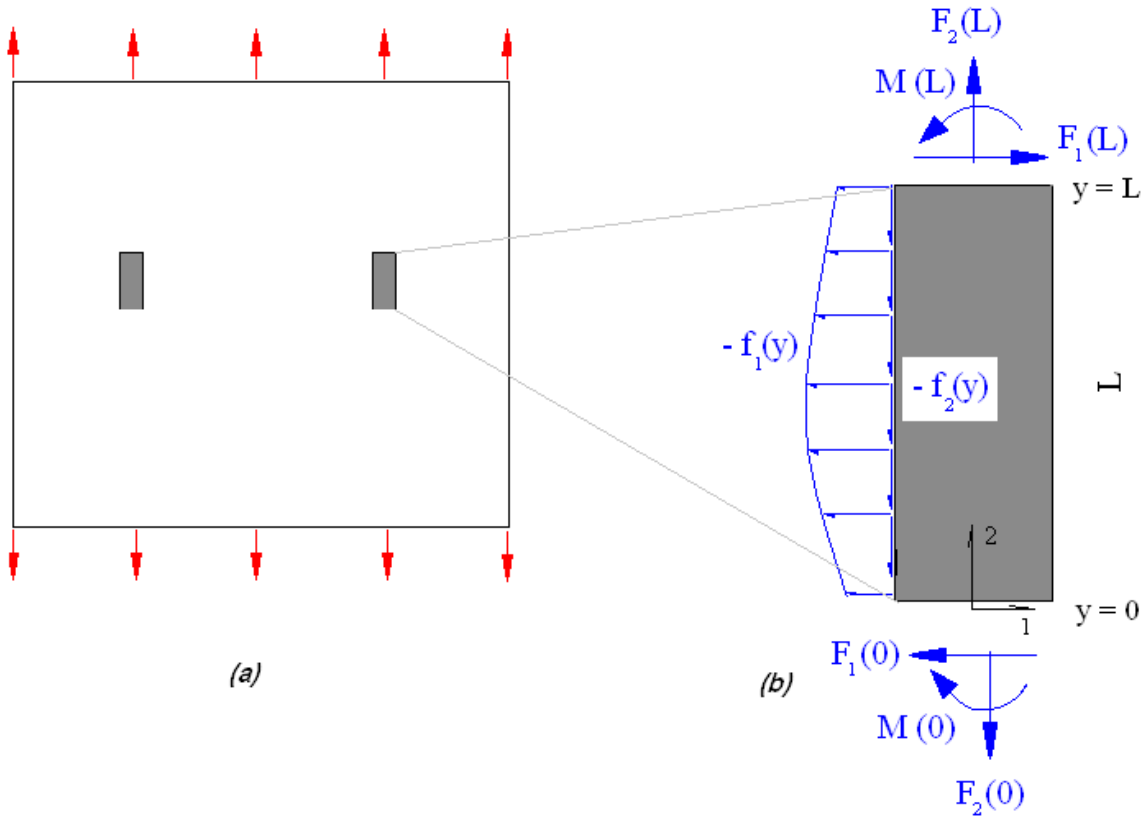

Figure 1 - (a) Plate with two sensors; (b) Forces e Momentums applied over the structure and sensors.

For the lateral direction (over the axe 1 in the figure) the differential equation of motion takes the form:

$$EJ\frac{\partial^4 u(y,t)}{\partial x^4}+\rho\frac{\partial^2 u(y,t)}{\partial t^2}=p(y,t) \tag{18}$$

If the load is harmonic

$$p(y,t)=p(y)\sin\omega t \tag{19}$$

where

$$p(y)=F_1(0)-F_1(L)+f_1(y) \tag{20}$$

Substituting eqs. (2) and (3) in eq. (1) and doing some simple rearrangement we get the following equation (Kolousek, 1973).

$$EJ\frac{d^4u(y)}{dy^4}+\rho\omega^2u(y)=p(y) \tag{21}$$

The general response, considering p(x) = 0 for the equation above is the following:

$$u(y)=A\cos{}^{\lambda y}\!/_{l}+B\sin{}^{\lambda y}\!/_{l}+C\cosh{}^{\lambda y}\!/_{l}+D\sinh{}^{\lambda y}\!/_{l} \tag{22}$$

with

$$\lambda=l\left(\frac{\rho\omega^2}{EJ}\right)^{1/4} \tag{23}$$

It must be consider also the particular solution for the equation (18), when it is considered the value of *p(y)*.

The integration constants are computed from the boundary conditions. In this case we consider an arbitrary rotation and displacement at the beginning and end of the beam. For our case we can use the following relations (Meriam and Kraige,1992):

$$-\frac{M(y)}{EJ}=u''(y) \tag{24}$$

and

$$-\frac{T(y)}{EJ}=u'''(y) \tag{25}$$

and from eq. (22) considering that the answer inside the stiffener has a linear variation, then the second and third derivatives are:

$$u''(y)=\frac{\lambda^2}{l^2}\left(-A\cos{}^{\lambda y}\!/_{l}-B\sin{}^{\lambda y}\!/_{l}+C\cosh{}^{\lambda y}\!/_{l}+D\sinh{}^{\lambda y}\!/_{l}\right) \tag{26}$$

and

$$u'''(y)=\frac{\lambda^3}{l^3}\left(A\sin{}^{\lambda y}\!/_{l}-B\cos{}^{\lambda y}\!/_{l}+C\sinh{}^{\lambda y}\!/_{l}+D\cosh{}^{\lambda y}\!/_{l}\right) \tag{27}$$

So using the conditions for the beginning and the end of the stiffener $y = 0$ and $y = L$ respectively we have:

$$A = \frac{M(0)}{EJ}\frac{l^2}{\lambda^2} + C \tag{28}$$

$$B = \frac{F_1(0)}{EJ}\frac{l^3}{\lambda^3} + D \tag{29}$$

$$C = \left[\frac{M(L)}{EJ}\frac{l^2}{\lambda^2} - \frac{F_1(0)}{EJ}\frac{l^3}{\lambda^3}\sin\lambda - \frac{M(0)}{EJ}\frac{l^2}{\lambda^2}\cos\lambda\right]\frac{1}{\cos\lambda - \cosh\lambda} - D\frac{\sin\lambda - \sinh\lambda}{\cos\lambda - \cosh\lambda} \tag{30}$$

$$D = \left[\frac{M(L)}{EJ}\frac{l^2}{\lambda^2} - \frac{F_1(0)}{EJ}\frac{l^3}{\lambda^3}\sin\lambda - \frac{M(0)}{EJ}\frac{l^2}{\lambda^2}\cos\lambda\right]\frac{(-\sin\lambda - \sinh\lambda)}{2(\cos\lambda\cosh\lambda - 1)} + \left[\frac{F_1(0)}{EJ}\frac{l^3}{\lambda^3} - \frac{M(0)}{EJ}\frac{l^2}{\lambda^2}\sin\lambda - \frac{F_1(L)}{EJ}\frac{l^3}{\lambda^3}\right]\frac{(\cos\lambda - \cosh\lambda)}{2(\cos\lambda\cosh\lambda - 1)} \tag{31}$$

For the longitudinal direction the differential equation takes the form.

$$E\,S\frac{\partial^2 v(y,t)}{\partial x^2} - \rho\frac{\partial^2 v(y,t)}{\partial t^2} - p(y,t) = 0 \tag{32}$$

If the load is harmonic

$$p(y,t) = p(y)\sin\omega t \tag{33}$$

where

$$p(y) = F_2(0) - F_2(L) + f_2(y) \tag{34}$$

Substituting eqs. (33) and (34) in eq. (32) and doing some simple rearrangement we get the following equation (Kolousek, 1973).

$$ES\frac{d^2 v(y)}{dy^2} + \rho\omega^2 v(y) = p(y) \tag{35}$$

The general response for the equation above is the following

$$v(x) = G\cos\psi\,y/l + H\sin\psi\,y/l \tag{36}$$

with

$$\psi = l\left(\frac{\rho\omega^2}{ES}\right)^{1/2} \tag{37}$$

The same procedure must be taken to determine the particular solution of the equation (12). The integration constants are also computed from the boundary conditions. For the case here we have the following relation:

$$\frac{N(y)}{ES} = v'(y) \tag{38}$$

and from eq. (19) the first derivative is:

$$v'(y) = \frac{\psi}{l}\left(-E\sin\psi\,y/l + F\cos\psi\,y/l\right) \tag{39}$$

So using the conditions for the beginning and the end of the stiffener $y = 0$ and $y = L$ respectively we have:

$$G = H\frac{\cos\psi}{\sin\psi} - \frac{F_2(L)}{ES}\frac{l}{\psi}\frac{1}{\sin\psi} \tag{40}$$

$$H = \frac{F_2(0)}{ES}\frac{l}{\psi} \tag{41}$$

5. PIEZOELECTRIC EFFECT

According to the IEEE compact matrix notation [7], the coupled electromechanical constitutive equations of a linear piezoelectric material are written as

direct piezoelectric effect: $D = \varepsilon^T E + d\sigma$ (42)

converse piezoelectric effect: $\varepsilon = s^E\sigma + d'E$ (43)

where D (charge/area) and E (voltage/length) are the electric displacement and electric field respectively. ε and σ are the mechanical strain and stress, d, ε^T and s^E are the piezoelectric strain constant, dielectric permittivity and compliance constant, respectively. The superscripts E and T indicate that the values of the constant are obtained at a constant electrical field and constant stress respectively.

For the sensor model, according to [8] and assuming that the sensor is sufficiently small to consider the strain constant inside the sensor area, the output voltage can be written as

$$V_{out} = \frac{d_3 E_p h_p \varepsilon_R}{4K_3 \varepsilon_0 \pi (1-\upsilon_p)} \tag{44}$$

where d_{31} is the piezoelectric charge coefficient equal to 130 x 10^{-12} m V^{-1}, E_p is the young modulus equal to 76 x 10^9, h_p is the thickness, K_3 is the relative dielectric constant equal to 1280, and $\varepsilon 0$ is the dielectric permittivity of a free space equal to 8.85 x 10^{-12} for PKI-402 piezoelectric sensor.

6. NUMERICAL EXAMPLES

In order to have some values of comparison, it will be shown similar examples as the executed in the reference [9 and 10]. There the uses of Lamb waves have shown that the crack can be detected, although some problems with blind zones are also addressed. Here the dynamic evaluation of the strain field in a plate will show another way of analysing the problem of crack detection.

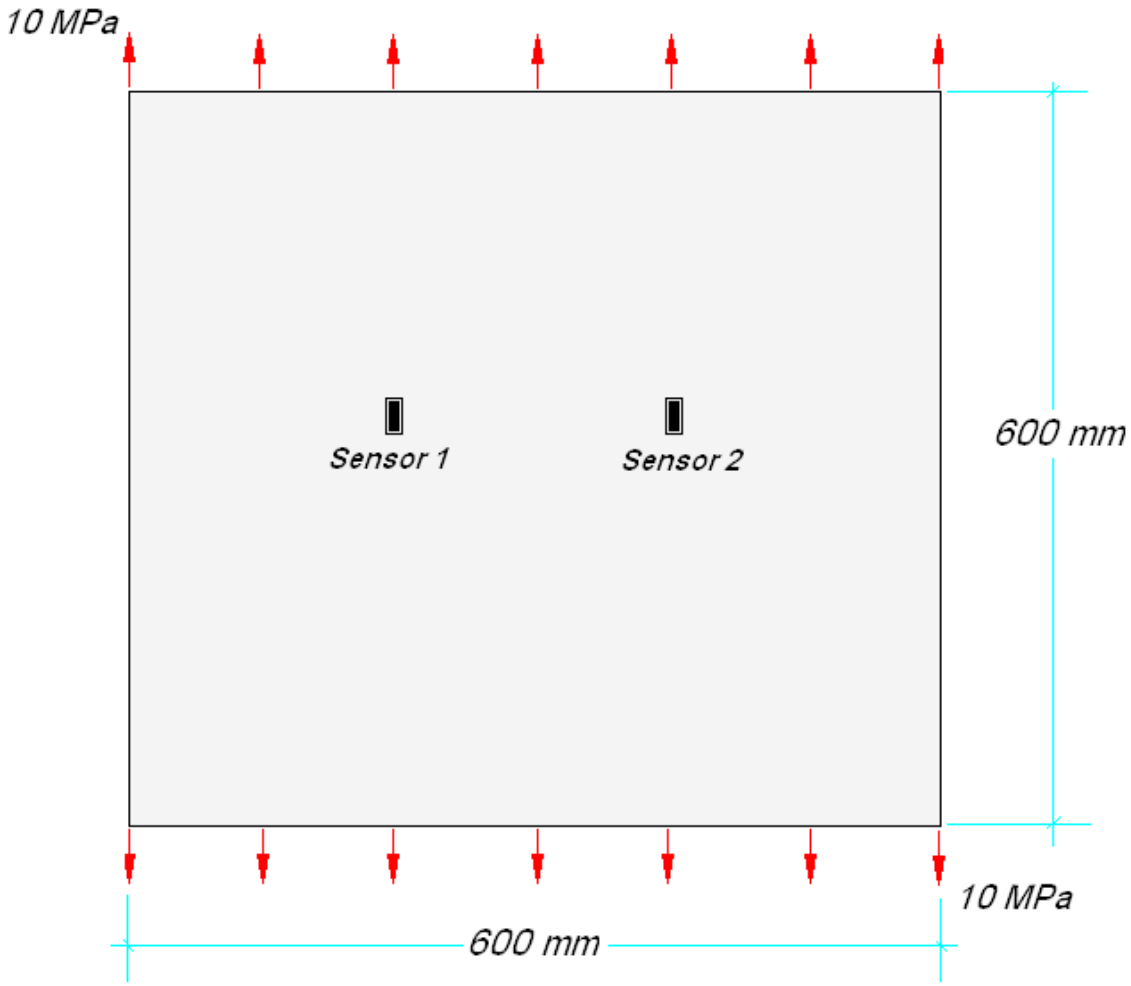

Figure 2 – Aluminium plate with 2 sensors.

The figure 2 shows the plate aluminium plate whose properties are given in table 1 and the configuration of the mesh used in the DBEM code, with 24 quadratics elements and 48 nodes.

Table 1 – Geometrical and material properties of aluminium plate.

Dimensions (mm^3)	600 x 600 x 2
Young's modulus, E (GPa)	72.5
Shear modulus, G (GPa)	27.25
Mass density, ρ ($kg\ m^{-3}$)	2700
Poisson Coefficient, υ	0.33

The table 2 shows the properties from the PZT sensors.

Table 2 – Geometrical and material properties of PZT – ceramic (PKI-402)

Dimensions (mm^3)	8 x 8 x 0.5
Young's modulus, E_p (GPa)	76
Shear modulus, G_p (GPa)	29
Mass density, ρ_p ($kg\ m^{-3}$)	7600
Poisson Coefficient, υ_p	0.31
Relative dielectric constant K_3	1280
Piezoelectric charge coefficient d_{31}, ($m\ V^{-1}$)	130×10^{-12}
Thickness, h (cm)	0.05
Dielectric permittivity of a free space, ε_0 ($F\ m^{-1}$)	8.85×10^{-12} $F\ m^{-1}$

The Figure 3 shows the results to the output voltage normalized by the value V0 which is the value for the same pristine state for plate in the static analysis.

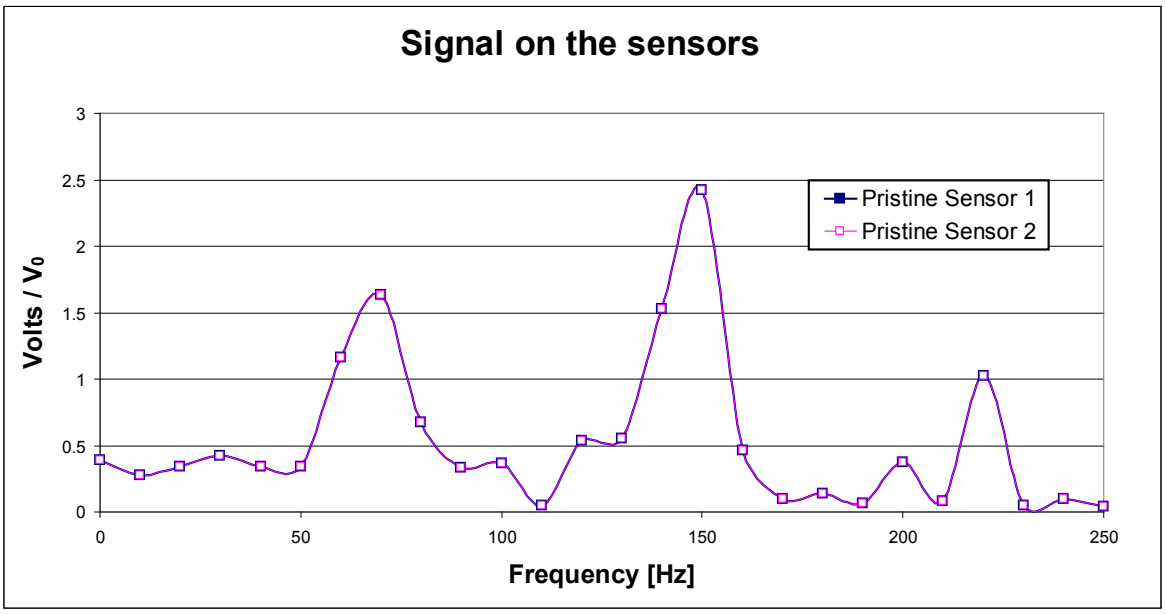

Figure 3 – Output for the pristine state of the plate.

7. DETERMINATION OF A CRACK IN A SQUARE ALUMINIUM PLATE

In all numerical example here presented it was adopted a coefficient of shear deformation from the adhesive from 0,085. Different values to this parameter can also be utilized if a comparison of the effect of such parameter was necessary. The Mesh of DBEM utilized was with 28 quadratic elements and 56 nodes for all cases in this first example.

It was used a straight crack from 4 mm which can be easily detected using the measurement of the dynamic strain field and the signal in the sensor increases with the proximity from the crack. The figure 4 shows two different positions for the crack. It can be seen in the figure 5 the increased signal detected in the sensors when there is a crack inside the plate. The curves for the first crack are equal for the both sensor because of the symmetry of the problem. But we can note that the signal increase for the first sensor when we approach the crack of it, and also can be noted that the signal decrease for the second sensor because the crack is becoming more distant of it.

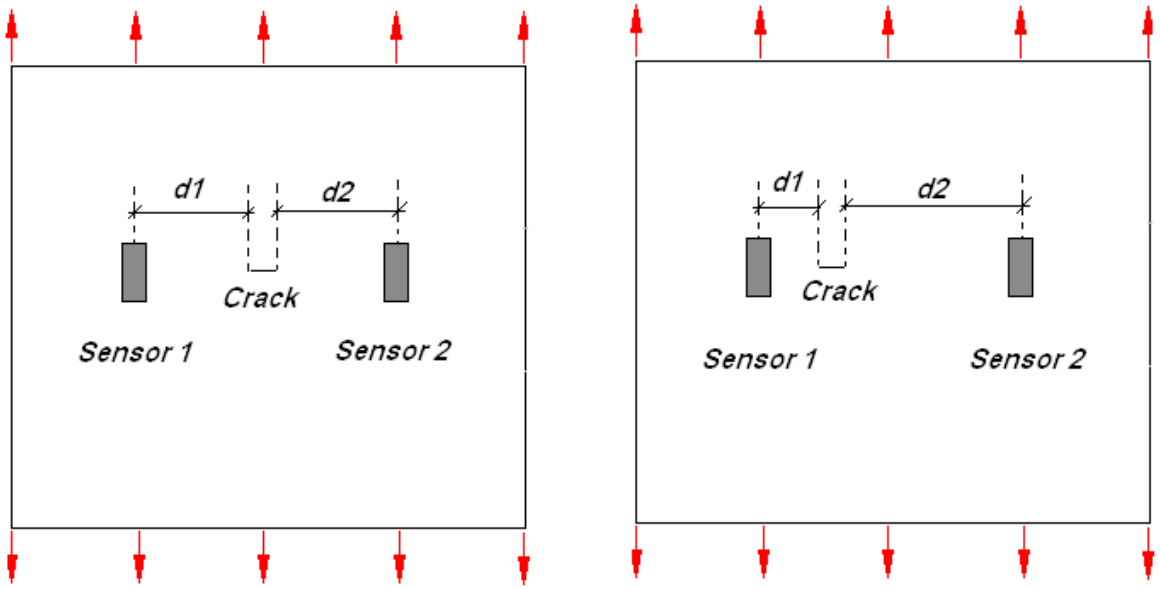

Figure 4 – Configuration of the problem with straight crack in the plate.

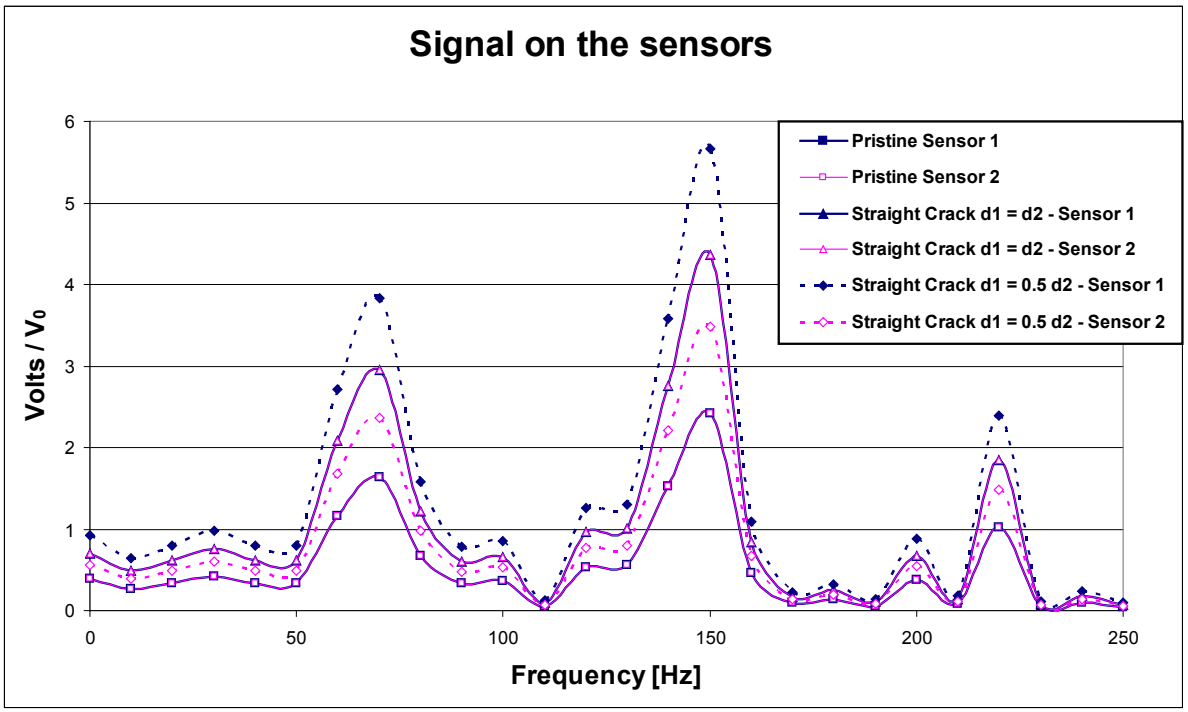

Figure 5 – Output from the sensors with straight cracks.

The figure 6 shows the problem for the case of a slant crack. The angle of inclination of the crack is for the case 45 degrees.

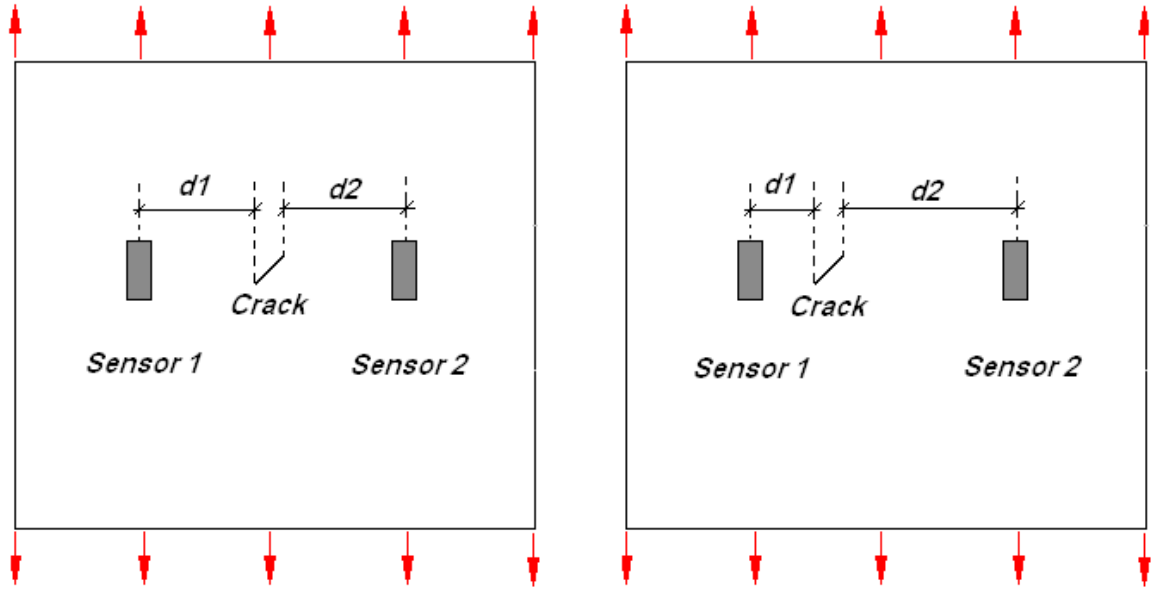

Figure 6 – Configuration of the problem with slant crack in the plate.

The graphic on the figure 7 shows the values from output for the slant crack. The behaviour is the same that for the straight crack, the only difference now is in the values of the output, in this case they are lower when compared with the straight crack because of the lower values of the deformations in the plate.

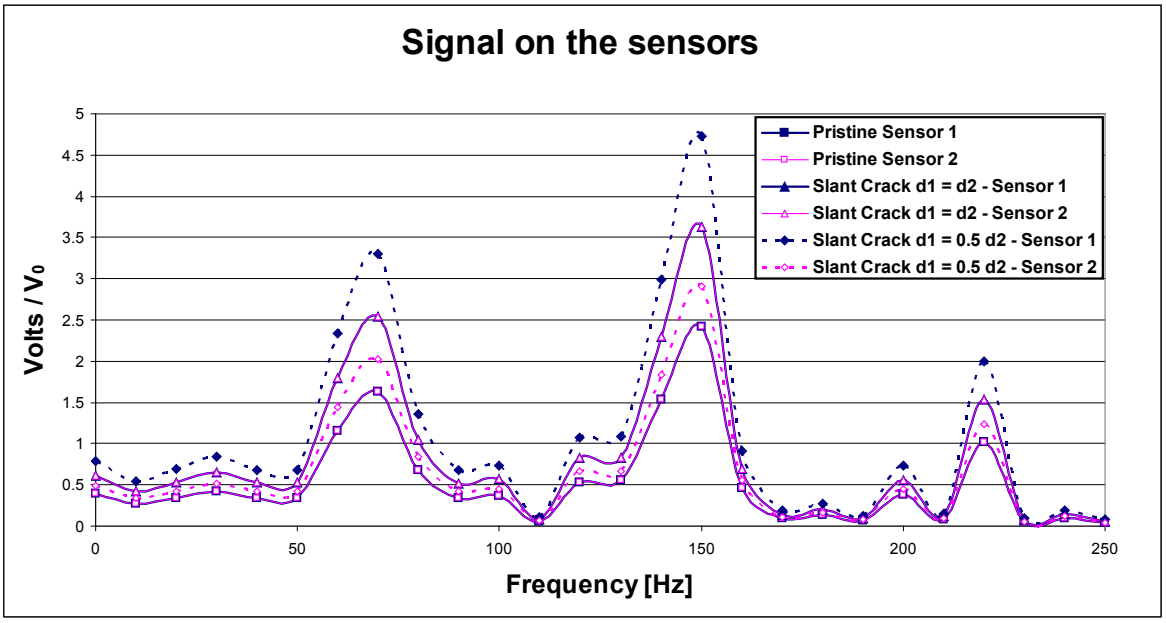

Figure 7 – Output from the sensors with slant cracks.

The last example is just for comparison between the values of the slant crack with the straight crack. Both cracks are positioned in the centre of the plate. The results can be seen in the figure 8.

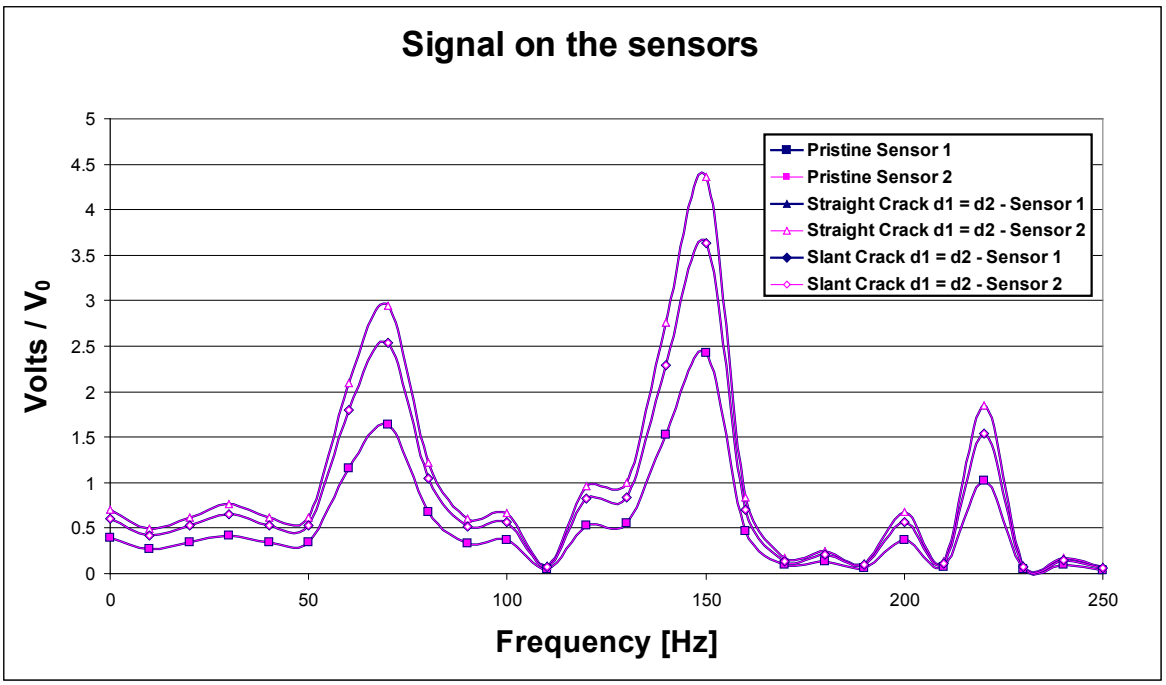

Figure 8 – Output from the sensors for straight and slant central crack.

8. CONCLUSIONS

The precisely computation of the dynamic strain field inside plates allowed by Dual Boundary Element Method using Laplace Transform permit us to propose a new methodology of health monitoring using the computation of dynamic strain fields. It was noted that the

strain field can show with great precision the behaviour of the cracks inside plates. This methodology could be used without the normally necessary neural networks used to do the heath monitoring of the plates.

9. ACKNOWLEDGEMENTS

The authors gratefully acknowledge CNPq (Brazilian National Research Council) and CAPES Foundation (Foundation for the Coordination of Higher Education and Graduate Training) for their support for this research.

REFERENCES

[1] W. Staszewski, C. Boller and G. Tomlinson "**Health Monitoring of Aerospace Structures – Smart Sensor Technologies and signal processing**" John Wiley & Sons, Ltd. England 2004.

[2] R. Ali, D. R. Mohapatra, and S. Gopalakrishnan "**Constrained piezoelectric thin film for sensing of subsurface cracks**" Smart Materials and Structures, 14, 376 – 386. 2005.

[3] M. H. Aliabadi and D. P. Rooke, "**Numerical Fracture Mechanics**" Solid Mechanics and its Applications, Computational Mechanics Publications. 1991.

[4] A. Portela, M. H. Aliabadi and D. P. Rooke, "**Dual boundary Element Method, effective implementation for crack problems**" International Journal of Numerical Methods in Engineering, 33, 1269 – 1287. 1992.

[5] N. K. Salgado and M. H. Aliabadi, "**The application of the Dual Boundary Element Method to the analysis of cracked stiffened panels**" Engineering Fracture Mechanics, 54, 1, 91 – 105. 1996.

[6] Y. C. Liang and C. Hwu, "**On-line identification of holes/cracks in composite structures**" Smart Materials and Structures, 10, 599 – 609. 2001.

[7] IEEE Piezoelectricity IEEE Standard 176. New York. 1978.

[8] X. Lin and F. G. Yuan, "**Diagnostic Lamb waves in an integrated piezoelectric sensor/actuator plate: analytical and experimental studies**" Smart Materials and Structures, 10, 907 – 913. 2001.

[9] P. S. Tua, S. T. Quek and Q. Wang, "**Detection of cracks in plates using piezo-actuated Lamb waves**" Smart Materials and Structures, 13, 643 – 660. 2004.

[10] S.P.L. Leme, M.H. Aliabadi, L.M. Bezerra, P. W. Partridge, "**Dual Boundary Element Method to Detect the Presence of Cracks and Growth Using Static Strain for Health Monitoring"** to be published.